IFSCC 2025 full paper (IFSCC2025-1106)

Oxidation of Metal-Phenolic Network on Rod-shaped Zinc Oxide for Broad-spectrum Sunscreen

Kyounghee Shin [1], Myunghee Lee [1], Saehan Cho [2], Rafia Tasnim Rahman [2], Jeonga Kim [2], Jin Woong Kim [3], Jongwon Shim [4] and Yoonsung Nam [5,*]

[1] R&D center, SUNJIN BEAUTY SCIENCE, Seoul; [2] Department of Materials Science and Engineering, Korea Advanced Institute of Science and Technology, Daejeon; [3] 3School of Chemical Engineering, Sungkyunkwan University, Suwon; [4] Department of Applied Chemistry, Dongduk Women's University, Seoul; [5] Department of Biological Science, Korea Advanced Institute of Science and Technology, Daejeon, Korea, South

1. Introduction

Inorganic ultraviolet (UV)-protective materials, particularly those based on wide bandgap metal oxides such as titanium dioxide (TiO_2) and zinc oxide (ZnO), have emerged as prominent alternatives to traditional organic UV filters. These materials offer intrinsic advantages due to their dual-action mechanism: they not only absorb high-energy UV photons via electronic transitions across their wide bandgaps, but also scatter incident light, thereby enhancing surface-level protection through physical reflection and refraction mechanisms [1,2]. This duality renders them especially attractive for broad-spectrum photoprotection across both UVA and UVB regions. The growing interest in these inorganic materials is closely tied to increasing regulatory and public scrutiny of conventional organic UV absorbers. Synthetic molecules such as oxybenzone and octinoxate have been implicated in potential endocrine-disrupting effects, allergic reactions, and environmental toxicity, particularly their detrimental impact on coral reef ecosystems [3]. As a result, mineral-based UV blockers are gaining traction not only for their photostability and lower systemic absorption but also for their perceived safety and environmental compatibility.

However, achieving optimal performance from metal oxide particles involves navigating a complex interplay between particle size, morphology, and surface chemistry. When the primary particle size exceeds approximately 150 nm, visible light scattering becomes dominant, resulting in undesirable optical whitening on the skin surface, an effect often referred to as the "white cast" [4,5]. This aesthetic drawback significantly limits user compliance and commercial acceptance, especially in facial sunscreen formulations where transparency is preferred. To reduce this whitening effect, researchers have explored nanosizing TiO_2 and ZnO particles, typically to dimensions below 100 nm. At this scale, the particles become nearly transparent in the visible range while still offering strong UV attenuation. However, this size reduction introduces a new concern: elevated photocatalytic

activity. As the surface-area-to-volume ratio increases, these nanomaterials can catalyze the generation of reactive oxygen species (ROS) upon UV exposure, including hydroxyl radicals and superoxide anions [6,7]. These ROS are capable of inducing oxidative stress in skin cells, accelerating lipid peroxidation, DNA damage, and inflammatory responses, thereby undermining the safety profile of the sunscreen formulation.

To address these challenges, precise engineering of particle properties is required. Strategies include surface modification through inert coatings, such as silica, alumina, or polymers, which act as physical barriers to electron-hole recombination, thereby reducing ROS formation without significantly impairing UV-blocking efficiency [8]. Additionally, hybridization with other functional nanomaterials or dopants can modulate electronic properties, suppress photocatalytic effects, and extend UV protection across a broader wavelength spectrum. Recent progress in nanomaterial synthesis has further refined these approaches. Techniques such as sol-gel encapsulation, atomic layer deposition, and surface ligand grafting have enabled fine-tuning of particle interface characteristics, enhancing dispersibility, stability, and biocompatibility [9–11]. As a result, next-generation inorganic sunscreens are increasingly able to offer transparent, photostable, and biologically inert formulations that meet the growing demand for safe and effective UV protection, both in dermatological and ecological terms.

Under mildly acidic conditions, zinc oxide (ZnO) exhibits a propensity to release Zn^{2+} ions through surface-mediated proton exchange mechanisms, wherein protons (H^+) from the surrounding environment displace loosely bound Zn^{2+} from the oxide lattice [12–14]. This ion-release process not only contributes to the dynamic surface chemistry of ZnO but also plays a role in buffering the local pH environment, especially in biological or slightly acidic systems. The underlying cause of this behavior lies in the relatively labile coordination of Zn^{2+} within the ZnO crystal structure, which permits facile dissociation in the presence of protons. Similar characteristics are observed in other divalent metal oxides, such as copper oxide (CuO) and magnesium oxide (MgO), which also demonstrate controlled ion liberation under acidic or physiological conditions due to their comparable metal–oxygen bond strengths and surface hydration behavior [12,15,16].

This controlled ion release can be strategically leveraged to drive the in situ formation of metal-phenolic networks (MPNs), enabling spontaneous coordination-driven assembly between the liberated Zn^{2+} ions and phenolic ligands without the need for externally added metal precursors. Such a self-sufficient mechanism simplifies the fabrication process and improves the spatial control of coating on ZnO surfaces. However, a notable distinction arises when comparing ZnO-based MPN systems with those involving TiO_2. In TiO_2 composites, ligand-to-metal charge transfer (LMCT) interactions between phenolic ligands and the Ti(IV) center can significantly alter the photophysical properties of the material—often extending its light absorption capability into the visible spectrum and enhancing photocatalytic or photoprotective performance [17,18]. As a result, the light absorption properties of ZnO nanoparticles and the MPN coating may function independently, which could limit their effectiveness in blocking high-energy visible (HEV) light. This underscores the need for

complementary approaches to improve HEV attenuation in MPN-coated ZnO particles (ZnO@MPN).

In this study, we present a facile, one-pot synthesis for constructing metal–phenolic network (MPN) coatings on ZnO particles to achieve effective shielding against both ultraviolet (UV) and high-energy visible (HEV) light. The process exploits tannic acid (TA), which plays a dual role: donating protons (H^+) to induce Zn^{2+} ion release from ZnO surfaces, and undergoing oxidation to form quinone intermediates that dimerize into stable MPNs. This pH-dependent route enables spontaneous MPN assembly without external metal ion precursors. To enhance HEV attenuation, we leverage the oxidative conversion of TA into quinone-rich chromophores, which exhibit characteristic brown coloration due to π-conjugated structures and extended light absorption into the HEV range [19–22]. At the ZnO@MPN junction, the release of Zn^{2+} generates surface vacancies that, in the presence of oxygen and moisture, can lead to reactive oxygen species (ROS) formation [23]. However, the oxidative transformation of TA, driven by ZnO lattice destabilization and H^+-induced electron transfer, results in a quinone-enriched coating that not only boosts HEV absorption but also suppresses photocatalytic ROS generation [20,24,25]. This strategy simultaneously improves the optical performance and biocompatibility of ZnO-based sunscreens, offering a viable path toward eco-friendly, broad-spectrum photoprotective formulations that overcome the limitations of conventional inorganic filters.

2. Materials and Methods

2.1. Materials

Rod-shaped ZnO particles (SUNZnO-200) were supplied by Sunjin Beauty Science, Seoul, Republic of Korea. Tannic acid, ensulizole (2-phenylbenzimidazole 5-sulfonic acid) and sodium hydroxide (NaOH) were procured from Sigma-Aldrich (St. Louis, MO, USA). 2-Hydroxyterephthalic acid (2-HTPA) was sourced from Tokyo Chemical Industry (Tokyo, Japan). Phosphate-buffered saline (PBS, pH 7.4) was obtained from Bioneer Corp. (Daejeon, Republic of Korea). All experiments utilized deionized water from a Milli-Q system.

2.2. Methods

*2.2.1. S*pontaneous MPN Formation on rod-shaped ZnO

Rod-shaped ZnO particles were suspended in 9.2 mL of PBS to achieve a 1 wt% concentration. Then, 20 mM tannic acid (TA) solution (0.8 mL) was added, and the suspension was vortexed for one minute. The resultant ZnO@MPN composites were collected by centrifugation at 10,000 g for 5 minutes at room temperature (25 °C), and subsequently freeze-dried for 24 hours.

2.2.2. Characterization

Transmission electron microscopy (TEM) was carried out using a Talos F200X (Thermo Fisher Scientific, MA, USA) operated at 200 kV. Fourier-transform infrared (FT-IR) spectroscopy was conducted using a Nicolet iS50 (Thermo Fisher Scientific, MA, USA). Absorption spectra were obtained using a UV–vis–NIR spectrometer (Lambda 1050,

PerkinElmer, CT, USA) with an integrated sphere. For simulated solar irradiation, a xenon light source (HAL-320 Solar Simulator, Asahi Spectra Co., Tokyo, Japan) under AM 1.5G conditions (1-sun) was used.

2.2.3. In-situ TA oxidization of ZnO@MPN Particles

To assess the influence of environmental humidity on the oxidation of galloyl groups, ZnO/MPN particles were incubated under both low-humidity, low-oxygen (humidity ~0%, vacuum) and ambient conditions (humidity ~40%, atmospheric pressure). Characterization using FT-IR, ^{13}C cross polarization magic-angle spinning NMR (^{13}C CPMAS NMR), and UV-vis spectroscopy was performed to verify the formation of oxidized TA-Zn complexes on the particle surfaces.

2.2.4. Sun Protection Factor and UVA Protection Factor Analyses

ZnO-based particles were dispersed in 1,3-butylene glycol (1,3-BG) at a concentration corresponding to 20 wt% ZnO (estimated from thermogravimetric analysis (TGA)). The formulations were uniformly coated onto sandblasted PMMA plates (47 × 47 × 1.5 mm, HelioScreen HD6 Plates, France). In vitro measurements of sun protection factor (SPF) and UVA protection factor (UVAPF) were taken by averaging UV transmission (290–400 nm) across five different points on each plate.

2.2.5. Photo-induced ROS Suppression Assay

To quantify hydroxyl radical generation, a standard curve was calculated using serial dilutions of 2-hydroxyterephthalic acid (2-HTPA). Specifically, 18.2 mg of 2-HTPA was first dissolved in 1 mL of 0.2 M NaOH and further diluted with deionized water. ZnO-based particles were each suspended in PBS and mixed with a 1 mM terephthalic acid solution in a 1:1 volume ratio. These mixtures were irradiated under simulated sunlight (1-sun) and centrifuged at 10,000 g for 5 minutes. Fluorescence was recorded at 434 nm (excitation at 320 nm) using a microplate reader.

2.2.6. Organic UV Filter Degradation Assay

A solution of ensulizole (8 µM) was prepared by dissolving it in PBS using a bath sonicator. ZnO-based samples were dispersed in PBS (1 mg/mL) and combined with the ensulizole solution with a 1:1 volume ratio. After stirring in the dark at 400 rpm to allow for adsorption equilibrium, the suspensions were irradiated under simulated sunlight (1-sun). Following irradiation, the mixtures were centrifuged at 10,000 g for 5 minutes. Remaining ensulizole concentrations in supernatant were determined using UV–vis absorption spectroscopy.

3. Results

3.1. Fabrication of ZnO@MPN Particles via Zn^{2+} Ion Release from ZnO

Figure 1 illustrates the synthesis of zinc oxide/metal-phenolic network (ZnO@MPN) particles using TA as a single-component polyphenol precursor. This method utilizes the inherent release of Zn^{2+} ions from ZnO, which consumes surrounding H^+ ions, thereby increasing the

local pH and promoting the oxidation and dimerization of TA, leading to MPN formation at the ZnO interface. ZnO is known to release Zn^{2+} ions under acidic conditions, leading to surface transformation to a Zn-OH [14,23]. TA can donate H^{+} ions to the ZnO surface, facilitating the release of Zn^{2+} ions. The deprotonated TA, rich in electrons, can transfer electrons to surrounding oxygen molecules, generating ROS and oxidizing to quinones, which subsequently dimerize to form dimerized TA (dTA) [20,26,27]. Furthermore, when TA is deprotonated, it can bind with Zn^{2+} ions released from ZnO, leading to the formation of MPNs. This ongoing coordination between the catechol and galloyl moieties of dTA and the free Zn^{2+} ions promotes the deposition of an MPN layer onto the ZnO surface. Experimentally, dispersing ZnO into a TA solution adjusted to around pH 7 triggers the rapid generation of ZnO@MPN particles within one minute, owing to the swift interaction between TA and Zn^{2+} ions.

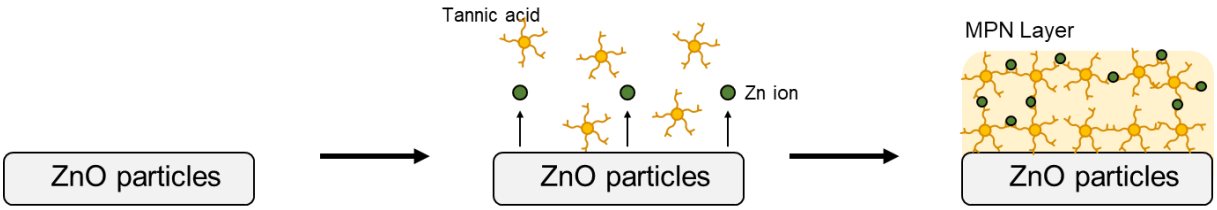

Figure 1. Schematic of the MPN formation of TA on the ZnO surface.

Transmission electron microscopy (TEM) analysis of bare ZnO (Figure 2a) and MPN-coated ZnO (ZnO@MPN, Figure 2b) confirms the formation of a conformal coating layer with a thickness of approximately 4–5 nm. This uniform MPN layer is attributed to the in situ coordination between liberated Zn^{2+} ions and polyphenolic ligands, which promotes consistent and homogeneous deposition on the particle surface.

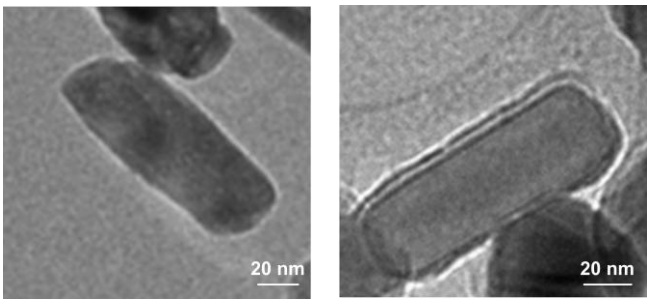

(a) (b)

Figure 2. TEM images of (a) ZnO and (b) ZnO@MPN.

3.2. Oxidation of dTA at the ZnO@MPN Interface

To improve the high-energy visible (HEV) light-shielding capability of ZnO@MPN particles, an oxidative modification strategy was employed, inspired by the natural browning mechanism in

fruits—where polyphenols undergo enzymatic oxidation upon exposure to air and moisture. In biological systems, this reaction is commonly mediated by polyphenol oxidase (PPO), which catalyzes the deprotonation and subsequent oxidation of polyphenols into quinone species. Analogously, at the ZnO@MPN interface, dTA can be oxidized to quinones via proton transfer to the ZnO surface and electron donation to ambient oxygen, as illustrated in Figure 3. The resulting quinonoid structures enhance π-electron delocalization, thereby broadening the absorption spectrum of the material to encompass the HEV light region.

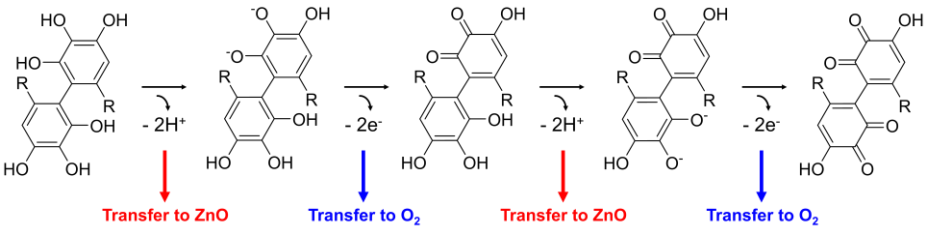

Figure 3. Schematic representation of the oxidation process of dTA at the ZnO surface.

Solid-state ^{13}C CPMAS NMR spectroscopy was performed to investigate chemical changes in polyphenols at the ZnO@MPN interface (Figure 4a). Pristine TA exhibited peaks at 91 ppm (C1 of glucose) and 70 ppm (C2–C5), along with signals from gallic acid units at 108–163 ppm [28,29]. In ZnO@MPN particles, a new peak at 111 ppm appeared, attributed to C–C coupling from gallic acid dimerization, while peaks at 108 ppm (C2*, C6*) decreased [30–32]. A signal at 147 ppm, corresponding to C–O–Zn coordination, was also observed, accompanied by reduced intensity in peaks associated with C3*, C4*, and C5* [29,33,34]. Notably, the brown ZnO@MPN particles formed via oxidation of dTA at the ZnO@MPN interface (ZnO@MPN(B)) exhibited a broad peak at 176–180 ppm, indicating quinone formation [35–37]. FT-IR analysis supported these findings (Figure 4b). ZnO@MPN particles showed characteristic TA peaks, including 1699 cm^{-1} (C=O), 1484 cm^{-1} (aromatic C=C), and 1342 cm^{-1} (phenolic O–H). In ZnO@MPN(B) particles, an additional band at 1630 cm^{-1}, corresponding to quinone C=O stretching, confirmed oxidation of dTA. Together, NMR and FT-IR results indicate that ZnO mediates polyphenol oxidation at the interface, forming a quinone-enriched MPN layer that enhances HEV light absorption through increased electron delocalization.

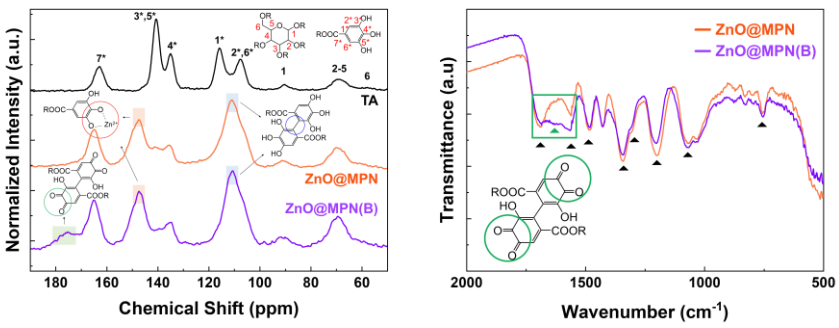

(a) **(b)**

Figure 4. (a) ^{13}C CPMAS NMR spectra of pristine TA, ZnO@MPN, and ZnO@MPN(B) particles indicating characteristic features corresponding to dimerization (blue), MPN formation (red), and oxidation (green). (b) FT-IR spectra of ZnO@MPN and ZnO@MPN(B) particles, indicating distinct peaks associated with the oxidation process.

4.3. UV-to-HEV Blocking Performance of ZnO@MPN Particles

UV–visible spectroscopy showed that pristine ZnO strongly absorbs in the UV region, with a sharp cutoff around 375 nm (Figure 5). ZnO@MPN particles exhibited extended absorption up to 420 nm due to dTA, along with weak absorption in the 400–800 nm range from metal–polyphenol complexation. ZnO@MPN(B) particles showed markedly increased absorption in the 400–600 nm range, attributed to dTA oxidation, and broader absorbance across 400–800 nm due to additional complexation during incubation..

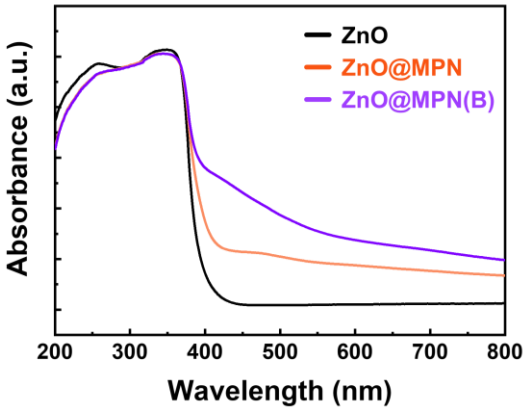

Figure 5. UV-visible absorption spectra of ZnO, ZnO@MPN, and ZnO@MPN(B) particles.

To assess the effect of broadened light absorption on photoprotection, ZnO, ZnO@MPN, and ZnO@MPN(B) particles were dispersed at 20 wt% in 1,3-BG and evaluated for SPF and UVAPF (Figures 6). Pristine ZnO showed SPF 8.5 and UVAPF 6.3. ZnO@MPN dispersions yielded approximately double these values. Remarkably, ZnO@MPN(B) dispersions exhibited SPF 26.4 and UVAPF 19.3, reflecting a threefold enhancement compared to unmodified ZnO. These findings demonstrate that MPN hybridization and subsequent oxidation significantly improve the UV and HEV light shielding efficacy of ZnO particles.

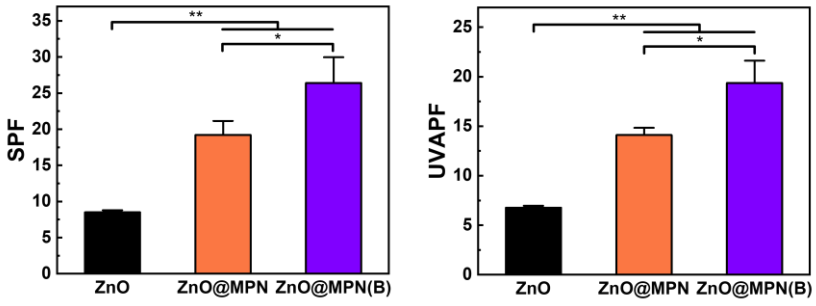

(a) (b)

Figure 6. (a) SPF and (b) UVAPF values for 20 wt% dispersions of each ZnO, ZnO@MPN, and ZnO@MPN(B) particles in 1,3-BG. Statistical significance is denoted as *p < 0.05 and **p < 0.0001.

4.4. Safety Evaluation of ZnO@MPN Particles for Sunscreen Applications

Hydroxyl radical generation under 1-sun exposure was used to assess these ZnO particles safety (Figure 7a). ZnO particles produced ~1 nmol h^{-1} of hydroxyl radicals, while ZnO@MPN and ZnO@MPN(B) showed >99% suppression over 3 hours, highlighting the MPN layer's ROS-blocking effect regardless of oxidation state. ROS also degrade UV filters. Ensulizole stability tests under simulated sunlight (Figure 7b) showed rapid degradation with ZnO (~15% remaining), whereas ZnO@MPN and ZnO@MPN(B) preserved ensulizole completely, confirming the MPN layer's protective role.

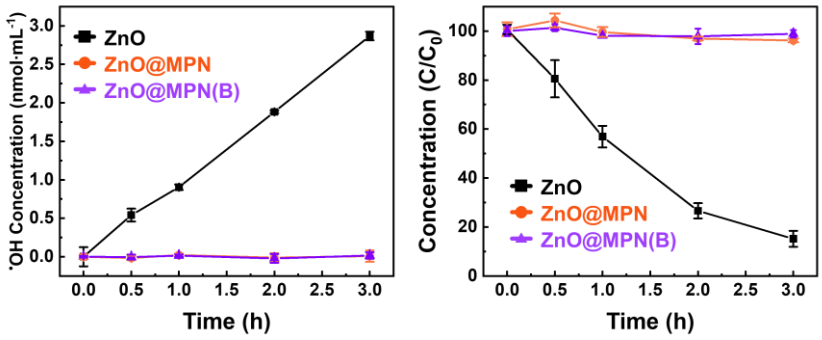

(a) (b)

Figure 7. Hydroxyl radical generation (a) and degradation of organic UV filters (b) by ZnO, ZnO@MPN, and ZnO@MPN(B) particles under 1-sun irradiation.

4. Discussion

We demonstrated a simple one-pot method to form and oxidize MPN coating on ZnO particles via spontaneous Zn^{2+} release. This process produced ZnO@MPN(B) particles with enhanced optical and suppressed photochemical properties. The MPN layer formed from tannic acid not only suppressed photoinduced ROS but also extended light absorption into the HEV range, particularly after oxidation to quinone structures. These changes significantly improved the sun protection performance, with ZnO@MPN(B) achieving threefold higher SPF and UVAPF values than pristine ZnO. Moreover, ZnO@MPN(B) effectively suppressed hydroxyl radical generation and prevented degradation of the organic UV filter, ensulizole, demonstrating its protective role in sunscreen formulations. Overall, this study highlights the potential of oxidized polyphenol coatings as a safe, scalable, and eco-friendly strategy to improve the performance of inorganic sunscreens.

5. Conclusion

In this study, we developed a simple and spontaneous one-pot method to create and oxidize an MPN coating on rod-shaped ZnO. The ZnO@MPN(B) particles showed notable improvements in both structure and optical properties. The MPN layer served two key functions: sta-

bilizing ROS and expanding optical absorption into the HEV region through oxidation-driven electron delocalization. This approach offers a promising path toward broad-spectrum, biocompatible photoprotection for cosmetic applications.

6. Acknowledgements

This research was supported by a grant of the Korea Health Technology R&D Project through the Korea Health Industry Development Institute (KHIDI), funded by the Ministry of Health & Welfare, Republic of Korea (grant number : RS-2024-00340429).

7. References

[1] T. A. Egerton, I. R. Tooley, *Int. J. Cosmet. Sci*. 2012, 34, 117.
[2] T. G. Smijs, S. Pavel, *Nanotechnol. Sci. Appl.* 2011, 4, 95
[3] Y. Huang, J. C. F. Law, T. K. Lam, K. S. Y. Leung, *Sci. Total Environ*. 2021, 755, 142486.
[4] M. J. Osmond, M. J. McCall, *Nanotoxicology* 2010, 4, 15.
[5] R. Wolf, D. Wolf, P. Morganti, V. Ruocco, *Clin. Dermatol.* 2001, 19, 452.
[6] S. Malato, P. Fernández-Ibáñez, M. I. Maldonado, J. Blanco, W. Gernjak, Catal. Today 2009, 147, 1.
[7] M. I. Setyawati, C. Y. Tay, D. T. Leong, *Small* 2015, 11, 3458.
[8] C. Surber, J. Plautz, S. Dähnhardt-Pfeiffer, U. Osterwalder, *Curr. Probl. Dermatology* 2021, 55, 203.
[9] S. Choi, R. T. Rahman, B. M. Kim, J. Kang, J. Kim, J. Shim, Y. S. Nam, *ACS Appl. Mater. Interfaces* 2024, 16, 16767.
[10] H. Y. Son, B. Il Koo, J. B. Lee, K. R. Kim, W. Kim, J. Jang, M. S. Yoon, J. W. Cho, Y. S. Nam, *ACS Appl. Mater. Interfaces* 2018, 10, 27344.
[11] A. Morlando, V. Sencadas, D. Cardillo, K. Konstantinov, *Powder Technol*. 2018, 329, 252.
[12] K. Donaldson, A. Schinwald, F. Murphy, W. S. Cho, R. Duffin, L. Tran, C. Poland, *Acc. Chem. Res.* 2013, 46, 723.
[13] X. Wang, T. Sun, H. Zhu, T. Han, J. Wang, H. Dai, *J. Environ. Manage.* 2020, 267, 110656.
[14] J. Liu, X. Feng, L. Wei, L. Chen, B. Song, L. Shao, *Crit. Rev. Toxicol.* 2016, 46, 348.
[15] W. S. Cho, R. Duffin, C. A. Poland, A. Duschl, G. J. Oostingh, W. MacNee, M. Bradley, I. L. Megson, K. Donaldson, *Nanotoxicology* 2012, 6, 22.
[16] Z. Yuan, Z. Wan, C. Gao, Y. Wang, J. Huang, Q. Cai, *J. Control. Release* 2022, 350, 360.
[17] K. R. Kim, S. Choi, C. T. Yavuz, Y. S. Nam, *ACS Sustain. Chem. Eng.* 2020, 8.
[18] S. Choi, J. Kim, R. T. Rahman, D. J. Lee, K. Lee, Y. S. Nam, *Chem. Eng. J.* 2022, 431, 133790.
[19] T. Tanaka, S. Watarumi, Y. Matsuo, M. Kamei, I. Kouno, *Tetrahedron* 2003, 59, 7939.
[20] T. S. Sileika, D. G. Barrett, R. Zhang, K. H. A. Lau, P. B. Messersmith, *Angew. Chem. Int. Ed. Engl.* 2013, 52, 10766.
[21] D. Tang, S. Chen, X. Liu, W. He, G. Yang, P. J. Liu, M. Gozin, Q. L. Yan, *Chem. Eng. J.* 2020, 381, 122747.
[22] X. Zhou, A. Iqbal, J. Li, C. Liu, A. Murtaza, X. Xu, S. Pan, W. Hu, *Antioxidants* 2021, 10, 1809.
[23] C. F. Liu, Y. J. Lu, C. C. Hu, *ACS Omega* 2018, 3, 3429.
[24] Y. Zhao, L. Xu, F. Kong, L. Yu, *Chem. Eng. J.* 2021, 416, 129090.

[25] H. Jafari, P. Ghaffari-Bohlouli, S. V. Niknezhad, A. Abedi, Z. Izadifar, R. Mohammadinejad, R. S. Varma, A. Shavandi, *J. Mater. Chem.* B 2022, 10, 5873.
[26] C. Zhang, Y. Ou, W. X. Lei, L. S. Wan, J. Ji, Z. K. Xu, *Angew. Chemie Int. Ed.* 2016, 55, 3054.
[27] D. Wu, J. Zhou, M. N. Creyer, W. Yim, Z. Chen, P. B. Messersmith, J. V. Jokerst, *Chem. Soc. Rev.* 2021, 50, 4432.
[28] T. J. Kim, J. L. Silva, M. K. Kim, Y. S. Jung, *Food Chem.* 2010, 118, 740.
[29] F. Weber, W. C. Liao, A. Barrantes, M. Edén, H. Tiainen, *Chem.-Eur. J.* 2019, 25, 9870.
[30] Z. Liu, W. J. C. De Bruijn, M. G. Sanders, S. Wang, M. E. Bruins, J. P. Vincken, *J. Agric. Food Chem.* 2021, 69, 2477.
[31] M. J. Chung, T. C. Chang, S. T. Chang, S. Y. Wang, *Holzforschung* 2021, 75, 91.
[32] G. H. Choi, M. G. Nam, S. J. Kwak, S. H. Kim, H. Chang, C. S. Shin, W. B. Lee, P. J. Yoo, *Energy Environ. Sci.* 2021, 14, 3203.
[33] D. F. Evans, A. M. Z. Slawin, D. J. Williams, C. Y. Wong, J. D. Woollins, *J. Chem. Soc. Dalt. Trans.* 1992, 0, 2383.
[34] E. Halevas, B. Mavroidi, O. Antonoglou, A. Hatzidimitriou, M. Sagnou, A. A. Pantazaki, G. Litsardakis, M. Pelecanou, *Dalt. Trans.* 2020, 49, 2734.
[35] R. Hollenstein, W. Von Philipsborn, Helv. Chim. Acta 1973, 56, 320.
[36] I. Melikhov, M. Bacher, T. Hosoya, H. Hettegger, A. Potthast, T. Rosenau, *Cellulose* 2023, 30, 5373.
[37] A. Ashraf, Y. Yue, T. Chen, S. Wang, Y. Zeng, *J. Mol. Struct.* 2024, 1313, 138659.